Unsteady Free magneto convective Heat and Mass Transfer in Newtonian Fluid Flow Past inclined porous plate with Radiation and viscous dissipation effects

Shamshuddin Md[1*], Sunder Ram M[2]

Abstract— In this article, a mathematical model is developed for magnetohydrodynamic (MHD), incompressible, dissipative and chemically reacting Newtonian fluid flow, heat and mass transfer through a porous medium from an inclined plate under the effect of thermal radiation was investigated numerically. Rosseland's diffusion approximation is used to describe the radiative heat flux in the energy equation. The governing partial differential equations for momentum, heat, and species conservation are transformed into dimensionless form under the assumption of low Reynolds number with appropriate dimensionless quantities. The emerging boundary value problem is then solved numerically with a Galerkin finite element method employing the weighted residual approach. The evolution of velocity, temperature and concentration are obtained as functions of the physical parameter of the problem studied in detail. The influence of many multi-physical parameters in these variables is illustrated graphically. Finally, grid independency is studied on different mesh (grid) sizes, which have been tabulated quantitatively. The study is relevant to MHD energy generators utilizing Newtonian working fluids and magnetic materials processing systems.

Index Terms— buoyancy, chemical reaction, inclined plate, Newtonian fluid, Thermal radiation, viscou dissipation, FEM.

1 INTRODUCTION

Magneto hydrodynamic (MHD) invoves the simulation flows in which electrically liquids or gases interact with an applied magnetic field. MHD is exploited in numerous modern industrial processes including, multi-physical magnetohydrodyna-mics [1] vortex control, ionized propulsion systems, MHD pumps, MHD accelerators, MHD generators [2], nuclear heat transfer control, medical treatment and energy generators. These systems are increasingly deploying or already feature more complex working fluids. Magneto-newtonian flows are therefore greatly relevant to such systems. Magnetohydrodynamic refers to the study of the mutual interaction of fluid flow with magnetic fields. Many investigators have examined boundary value problems of such fluids in recent years using a range of computational solvers. These include Postelnicu [3], Hayat *et al.* [4] and Mohamed et al., [5] whose used numerical and analytical methods, Alao *et al.* [6] who used spectral relaxation method, Ali *et al.* [7] who employed homotopy methods, Ahmed et al. [8] who employed finite difference method. A numerical solution of unsteady MHD convection heat and mass transfer past a semi-infinite vertical porous moving plate by adopting Element free Gelerkin method was studied by Sharma *et al.* [9], Helmy [10] studied unsteady free convection flow through a vertical porous plate. MHD Stokes problem for a vertical plate under the effects of mass transfer and free convection with transversely applied magnetic field was analyzed by Soundalgekar *et al.* [11]. Recently Umamaheshwar *et al.* [12] analyzed MHD transient free convection of a Newtonian fluid through infinite vertical porous plate also by incorporating thermal diffusion effects on unsteady free convection flow with magnetic field fixed relative to the fluid or plate was studied by Rushi kumar *et al*. [13].

Convective boundary layer flow problems in the cases of horizontal and vertical flat plates have been investigated quite extensively. The boundary layer flows adjacent to inclined plates or wedges have received less attention. The heat and mass transfer through an inclined plate received much attention because of its applications in engineering devices. An extensive review on various aspects of convective flows over inclined geometries has been made. Early studies related to the convection flow about an inclined surface in which the combined forced and free boundary layer problem has been discussed using the similarity method which was studied by Sparrow *et al.,* [14]. Later many researchers extended their ideas in different surfaces such as, vertical plate is considered by Gebhert and Pera [15] and on inclined plate by Chen and Yuh [16]. Other related works is Chamkha [17], Singh [18], Cheng [19] and Chen [20].

The current study is relevant to high temperature electromagnetic rheological flows in energy generators and magneto-rheological materials fabrication systems, where thermal radiation heat transfer is also significant. Radiation effects play an important role and that cannot be ignored [21,22], a few examples where high temperature heat transfer occur are gas turbines, nuclear power plants, missiles, satellites and space vehicles. Using Laplace technique, Heat and mass transfer effects on moving plate by incorporating Thermal radiation was examined by Muthukumara swamy [23]. In the most of investigations, the viscous dissipation term is conventionally neglected on the premise that under normal conditions the Eckert number is small based on an order of magnitude analysis. The effect which bears a great importance on heat transfer is viscous dissipation. When the viscosity of the fluid is high, the dissipation term becomes important. For many cases, such

as polymer processing which is operated at a very high temperature, viscous dissipation cannot be neglected, which is a possible factor in the design of large diameter oil pipe line under arctic environment, geothermal energy systems, hence study of viscous dissipation is important in various physical problems. Gebhert [24] investigated the effects of viscous dissipation in natural convection. Costa [25] has analyzed the thermodynamics of natural convection in enclosures with viscous dissipation. Gnaneswara and Bhaskar [26] investigated the radiation and mass transfer effects on an unsteady MHD free convection flow past a heated vertical porous plate with viscous dissipation. First-order irreversible chemical reaction which takes place both in the bulk of the fluid (homogeneous) as well as at plate which is assumed to be catalytic to chemical reaction. Although chemical reactions generally fall into one of two categories i.e. *homogenous* or *heterogenous*, the former is of interest in the present study. Homogenous chemical reactions take place uniformly throughout a given phase and are similar in nature to an internal source of heat generation. We consider the destructive type of homogenous chemical reaction. Recent advances in understanding the physics of flows and modeling the computational flow make tremendous contributions in Newtonian as well as non-Newtonian fluids of chemical engineering, this include Sivaiah and Srinivasa Raju [27], Babu and Satya Narayan [28], Nandkeolyar *et al.* [29], Seth *et al*, [30] and Sheri and Shamshuddin [31,32].

In the present investigation, we generalize and extend existing studies [12] to consider the combined effects of Thermal radiation and viscous dissipation on magnetohydrodynamic Newtonian fluid flow, heat and mass transfer from an inclined plate adjacent to a porous medium. The non-dimensional conservation equations are solved with a Galerkin finite element method. The effect of various physical parameters on the velocity, temperature and concentration profiles is illustrated graphically. Grid independency study has been carried out for different mesh sizes to show the results are independent of grid size. The current study is relevant to high temperature electromagnetic rheological flows in energy generators and magneto-rheological materials fabrication systems (where thermal radiation heat transfer is also significant) and has not appeared in technical literature thus far.

2 Mathematical Formulation

Consider a laminar boundary layer flow of a viscous incompressible, electrically conducting, chemically reacting Newtonian fluid past a semi-infinite moving permeable plate inclined at an angle α in vertical direction embedded in a homogeneous, isotropic, porous medium under the influence of thermal radiation and viscous dissipation were analyzed. The physical configuration is illustrated in Fig. 1. Darcy's law is assumed and low Reynolds number flow (viscous dominated). The positive x' coordinate is measured along the plate in the direction of fluid motion and the positive y' coordinate is measured perpendicular to the plate. Both wall temperature and concentration vary with the distance along the plate and they are always greater than their uniform ambient values existing far from the plate surface. A uniform magnetic field is assumed to be strong Bo is applied in the positive y' direction transversely to the plate. The applied magnetic field is assumed to be strong enough so that the induced magnetic field due to the fluid motion is weak and can be neglected.

This assumption is physically justified for partially ionized fluids and metallic liquids because of their small magnetic Reynolds number (Cramer and pai [33]). The fluid considered being gray, absorbing-emitting but non-scattering medium and rosseland approximation is used to describe the radiative heat flux. The radiative heat flux in the x' direction is considered negligible in comparison with that of y' direction. The Newtonian fluid contains a species which is reactive and obeys first order chemical reaction. Initially, the fluid as well as plate at rest which is maintained at temperature $T'_w > T'_\infty$ but for time $t' > 0$,the plate is linearly accelerated with increasing time in its own plane about the y' axis and temperature decreases with temperature $T' = 1/(1 + a\,t')$. It is assumed that the plate is infinite in extent and hence all physical quantities depends only on y' and t' only.

The general case is however greatly simplified for two-dimensional flows, as considered here. With these foregoing assumptions, the governing equations under Boussinesq approximation can be written in a Cartesian of reference as follows:

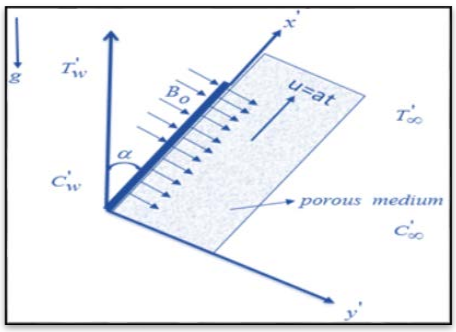

Fig 1: Geometry and coordinate system of the problem

$$\frac{\partial u'}{\partial t'} = \nu \frac{\partial^2 u'}{\partial y'^2} + g\beta_T \left(T'_w - T'_\infty\right) cos(\alpha) + g\beta_C \left(C'_w - C'_\infty\right) cos(\alpha) - \frac{\nu\, u'}{k'} - \frac{\sigma B_0^2 u'}{\rho} \quad (1)$$

$$\rho C_p \left(\frac{\partial T}{\partial t'}\right) = \kappa \frac{\partial^2 T}{\partial y'^2} - \frac{\partial q_r}{\partial y'} - Q'\left(T'_w - T'_\infty\right) + \mu \left(\frac{\partial u'}{\partial y'}\right)^2 \quad (2)$$

- *Shanshuddin MD, Depatment of Mathematics, Vaagdevi college of engineering (UGC autonomous), Warangal, Telangana state, India, PH-09866826099. E-mail: shammaths@gmail.com*
- *Sunder ram M, Depatment of Mathematics, Chaitanya Degree colleges (autonomous), Warangal, Telangana state, India, E-mail: msram70@gmail.com*

$$\frac{\partial C}{\partial t'} = D_m \frac{\partial^2 C}{\partial y'^2} - K_C\left(C'_w - C'_\infty\right) \tag{3}$$

Where u', v' velocity components along x', y' β_T and β_C are coefficient of thermal expansion and concentration expansion. ρ is the density of fluid, ν is the kinematic viscosity, K is permeability of porous medium, σ is the electrical conductivity of the fluid, g is the acceleration due to gravity, T'_w, T'_∞ are temperature of fluid at boundary layer and far away from surface. k is thermal conductivity of the medium. C_p is specific heat at constant pressure p, q_r is the radiative heat flux in y' direction, C'_w, C'_∞ are concentration of the solute and far away from surface. D_m is the molecular diffusivity, κ is the thermo diffusion ratio and K_c is the first order chemical reaction parameter.

The following are the spatial and temporeial boundary conditions

$$\left.\begin{aligned} &y', t' \le 0 : u' = 0,\ T'_w = T'_\infty,\quad C'_w = C'_\infty \\ &t' > 0 :\quad u' = U_0\, a'\, t', T'_w = T'_\infty + \left(\frac{T'_w - T'_\infty}{1 + At'}\right), \\ &\qquad C'_w = C'_\infty + \left(\frac{C'_w - C'_\infty}{1 + At'}\right) \quad at \quad y' = 0 \\ &\qquad and \\ &\qquad u' \to 0,\quad T'_w = T'_\infty,\ C'_w = C'_\infty,\ as\ y' \to \infty \end{aligned}\right\} \tag{4}$$

Where $A = U_0^2 / \nu$, U_0 is the plate velocity, a' is accelerated plate velocity. The local radiant for the case of an optically thin gray gas (Cogley *et al.* [34]) and radiative heat flux is given by

$$\frac{\partial q_r}{\partial y'} = -4a^*\sigma\left(T'^4_\infty - T'^4\right) \tag{5}$$

Where σ is Stefan–Boltzmann constant and a^* is the Mean absorption coefficient. Equation. (5) results in a highly nonlinear energy equation in T and it is difficult to obtain its solution. However, researchers have obtained this problem in past by assuming small temperature differences with in the fluid flow ([35], [36]). In this situation, Rosseland formula can be linearized about ambient temperature T'_∞ assuming that the difference in the temperature with in the flow such that T'^4 can be expressed as linear combination of the temperature, using Taylor's series expansion about T'_∞ the expansion of T'^4 can be written as follows

$$T'^4 = T'^4_\infty + 4T'^3_\infty\left(T' - T'_\infty\right) + 6T'^2_\infty\left(T' - T'_\infty\right)^2 + \ldots\ldots \tag{6}$$

Neglecting higher order terms beyond the first degree in $\left(T' - T'_\infty\right)$, we have

$$T^4 \cong 4T'^3_\infty T - 3T'^4_\infty \tag{7}$$

In view of equation (5) and (7) the basic equation (2) can be written as

$$\rho C_p\left(\frac{\partial T}{\partial t'}\right) = \kappa\frac{\partial^2 T}{\partial y'^2} + 16a^*\sigma T'^3_\infty\left(T'_\infty - T'\right) - Q'\left(T'_w - T'_\infty\right) + \mu\left(\frac{\partial u'}{\partial y'}\right)^2 \tag{8}$$

Let us introduce the following dimensionless variables:

$$\left.\begin{aligned} &u = \frac{u'}{U_0},\quad y = \frac{y'U_0}{\nu}, t = \frac{t'U_0^2}{\nu}, \theta = \frac{T' - T'_\infty}{T'_w - T'_\infty}, \phi = \frac{C' - C'_\infty}{C'_w - C'_\infty}, \\ &Gr = \frac{vg\beta_T(T'_w - T'_\infty)}{U_0^3}, Gm = \frac{vg\beta_C(C'_w - C'_\infty)}{U_0^3}, \\ &M = \frac{B_0^2}{U_0^2}\frac{\sigma\nu}{\rho}, K = \frac{k'U_0^2}{\nu^2}, Pr = \frac{\mu C_p}{\kappa}, Q = \frac{Q'\nu^2}{\kappa U_0^2}, Sc = \frac{\nu}{D_m}, \\ &F = \frac{16a^*\nu^2\sigma T'^3_\infty}{\kappa U_0^2}, Ec = \frac{U_0^2}{C_p(T'_w - T'_\infty)}, \gamma = \frac{K_c\nu}{U_0^2}. \end{aligned}\right\} \tag{9}$$

In view of equation (9) the basic field equations (1)- (3) can be expresswed in non-dimensional form as

$$\frac{\partial u}{\partial t} = \frac{\partial^2 u}{\partial y^2} + Gr\theta\cos(\alpha) + Gm\phi\cos(\alpha) - \left(M + \frac{1}{K}\right)u \tag{10}$$

$$\frac{\partial \theta}{\partial t} = \frac{1}{Pr}\frac{\partial^2 \theta}{\partial y^2} - \frac{1}{Pr}(F + Q)\theta + Ec\left(\frac{\partial u}{\partial y}\right)^2 \tag{11}$$

$$\frac{\partial \phi}{\partial t} = \frac{1}{Sc}\frac{\partial^2 \phi}{\partial y^2} - \gamma\phi \tag{12}$$

Where Gr, Gm, M, K, P_r, F, Q, Ec, Sc, γ denotes the Grashof number, Modified Grashof number, Magnetic field parameter, Permeability of the porous medium, Prandtl number, Thermal radiation parameter, Heat absorption parameter, Viscous dissipation, Schmidt number and Chemical reaction parameters respectively.

The corresponding initial and boundary conditions in dimensionless form are

$$\left.\begin{aligned} &y, t \le 0 : u = 0,\ \theta = 0,\quad \phi = 0 \\ &t > 0 :\quad u = a\,t,\ \theta = \frac{1}{1+t}, \phi = \frac{1}{1+t} \quad at \quad y = 0 \\ &\qquad and \\ &\qquad u \to 0,\quad \theta \to 0,\ \phi \to 0,\quad as\ y \to \infty \end{aligned}\right\} \tag{13}$$

3 NUMERICAL SOLUTION OF FINITE ELEMENT

METHOD

3.1 Finite element method

The finite element method is a most powerful technique for solving ordinary differential or Partial differential equations as well as for integral equations. This method is so general that it can be applied to a wide variety of engineering problems including heat transfer, fluid mechanics, ,solid mechanics, bio-fluid dynamics, geomechanics, chemical processing and in many other fields. The set of Partial differential equations (10)-(12) subject to boundary conditions (13) are nonlinear, coupled and therefore it cannot be solved analytically. Hence, the following Bathe [37] and Reddy [38], the finite element method is used to obtain an accurate and efficient solution to the boundary value problem under consideration. A review of the superior efficiency of FEM in hydromagnetic transport phenomena simulations compared with other numerical methods (e.g., boundary elements, finite volumes, smoothed particle hydrodynamics, network simulation, and spectral methods) has been provided by many investigators. The fundamental steps involved in the finite-element method are

- *Discretization of the infinite fluid domain into finite elements*
- *Derivation of element equations*
- *Assembly of elemnt equations*
- *Imposition of boundary conditions*
- *Solutionof ssembeled equations*

The final assembled equations so obtained can be solved by iterative technique. For computational purpose, the coordinate y is varied from 0 to $y_{max} = 10$,where y_{max} represents infinity i.e., external to the momentum, energy and concentration edge layers.

3.2 Variational Formulation

The variational formulation associated with equations (10) – (12) over a typical two -noded linear element (y_e, y_{e+1}) is given by

$$\int_{y_e}^{y_{e+1}} w_1\left[\left(\frac{\partial u}{\partial t}\right)-\left(\frac{\partial^2 u}{\partial y^2}\right)+Nu-\left(Gr\theta+Gm\phi\right)\cos\alpha\right]dy=0 \quad (14)$$

$$\int_{y_e}^{y_{e+1}} w_2\left[\left(\frac{\partial \theta}{\partial t}\right)-\frac{1}{Pr}\left(\frac{\partial^2 \theta}{\partial y^2}\right)+\frac{1}{Pr}\left(F+Q\right)\theta-Ec\left(\frac{\partial u}{\partial y}\right)^2\right]dy=0 \quad (15)$$

$$\int_{y_e}^{y_{e+1}} w_3\left[\left(\frac{\partial \phi}{\partial t}\right)-\frac{1}{Sc}\left(\frac{\partial^2 \phi}{\partial y^2}\right)+\gamma\,\phi\right]dy=0 \quad (16)$$

Where w_1, w_2, w_3 are the arbitrary test functions and may be viewed as the variation in u, θ and ϕ respectively. After reducing the order of integration and non – linearity, we arrive at the following system of equations.

$$\int_{y_e}^{y_{e+1}}\left[\left(w_1\right)\left(\frac{\partial u}{\partial t}\right)+\left(\frac{\partial w_1}{\partial y}\right)\left(\frac{\partial u}{\partial y}\right)+N\left(w_1\right)u-\left(w_1 Gr\,\theta+w_1 Gm\,\phi\right)\cos\alpha\right]dy \quad (17)$$
$$-\left[\left(w_1\right)\left(\frac{\partial u}{\partial y}\right)\right]_{y_e}^{y_{e+1}}=0$$

$$\int_{y_e}^{y_{e+1}}\left[\begin{array}{l}\left(w_2\right)\left(\frac{\partial \theta}{\partial t}\right)-\frac{1}{Pr}\left(\frac{\partial w_2}{\partial y}\right)\left(\frac{\partial \theta}{\partial y}\right)+\frac{1}{Pr}\left(w_2\right)\left(F+Q\right)\theta\\ -E_C\left(w_2\right)\left(\frac{\partial \bar{u}}{\partial y}\right)\left(\frac{\partial u}{\partial y}\right)\end{array}\right]dy \quad (18)$$
$$-\left[\left(\frac{w_2}{Pr}\right)\left(\frac{\partial \theta}{\partial y}\right)\right]_{y_e}^{y_{e+1}}=0$$

$$\int_{y_e}^{y_{e+1}}\left[\left(w_3\right)\left(\frac{\partial \phi}{\partial t}\right)+\frac{1}{Sc}\left(\frac{\partial w_3}{\partial y}\right)\left(\frac{\partial \phi}{\partial y}\right)+\gamma\left(w_3\right)\phi\right]dy \quad (19)$$
$$-\left[\left(\frac{w_3}{Sc}\right)\left(\frac{\partial \phi}{\partial y}\right)\right]_{y_e}^{y_{e+1}}=0$$

3.3 Finite Element Formulation

The finite element model may be obtained from equations (17) – (19) by substituting finite element approximations of the form:

$$u=\sum_{j=1}^{2} u_j^e\psi_j^e,\ \theta=\sum_{j=1}^{2}\theta_j^e\psi_j^e,\ \phi=\sum_{j=1}^{2}\phi_j^e\psi_j^e \quad (20)$$

With $w_1 = w_2 = w_3 = \psi_j^e$ $(i = 1, 2)$, where u_j^e, θ_j^e and ϕ_j^e are the velocity, temperature and concentration respectively at the jth node of typical e^{th} element (y_e, y_{e+1}) and ψ_i^e are the shape functions for this element (y_e, y_{e+1}) and are taken as:

$$\psi_1^e=\frac{y_{e+1}-y}{y_{e+1}-y_e} \text{ and } \psi_2^e=\frac{y-y_e}{y_{e+1}-y_e},\ y_e\le y\le y_{e+1} \quad (21)$$

The finite element model of the equations for e^{th} element thus formed is given by

$$\begin{bmatrix}K^{11} & K^{12} & K^{13}\\ K^{21} & K^{22} & K^{23}\\ K^{31} & K^{32} & K^{33}\end{bmatrix}\begin{bmatrix}u^e\\ \theta^e\\ \phi^e\end{bmatrix}+\begin{bmatrix}M^{11} & M^{12} & M^{13}\\ M^{21} & M^{22} & M^{23}\\ M^{31} & M^{32} & M^{33}\end{bmatrix}\begin{bmatrix}u'^e\\ \theta'^e\\ \phi'^e\end{bmatrix}=\begin{bmatrix}b^{1e}\\ b^{2e}\\ b^{3e}\end{bmatrix} \quad (22)$$

Where $[K^{mn}]$, $[M^{mn}]$ and $\{u^e\}$, $\{\theta^e\}$, $\{\phi^e\}$, $\{u'^e\}$, $\{\theta'^e\}$, $\{\phi'^e\}$ $\{b^{me}\}$ (m, n=1,2,3) are the set of matrices of order 2×2 and 2×1 respectively and $'$ (dash) indicates d/dy. These matrices are defined as follows:

$$\begin{cases} K_{ij}^{11} = \int_{y_e}^{y_{e+1}} \left[\left(\frac{\partial \psi_i^e}{\partial y} \right) \left(\frac{\partial \psi_j^e}{\partial y} \right) \right] dy, \\ K_{ij}^{12} = N \int_{y_e}^{y_{e+1}} \left[\left(\psi_i^e \right) \left(\psi_j^e \right) \right] dy, \\ K_{ij}^{13} = -\left[Gr + Gm \right] \cos \alpha \int_{y_e}^{y_{e+1}} \left(\psi_i^e \right) \left(\psi_j^e \right) dy, \\ M_{ij}^{11} = \int_{y_e}^{y_{e+1}} \left(\psi_i^e \right) \left(\psi_j^e \right) dy, \; M_{ij}^{12} = M_{ij}^{13} = 0 \end{cases} \tag{23}$$

$$\begin{cases} K_{ij}^{21} = 0, \; K_{ij}^{22} = -\frac{1}{Pr} \int_{y_e}^{y_{e+1}} \left[\left(\frac{\partial \psi_i^e}{\partial y} \right) \left(\frac{\partial \psi_j^e}{\partial y} \right) \right] dy \\ + \frac{1}{Pr} \left(F + Q \right) \int_{y_e}^{y_{e+1}} \left[\left(\psi_i^e \right) \left(\psi_j^e \right) \right] dy, \\ K_{ij}^{23} = -\left(Ec \right) \int_{y_e}^{y_{e+1}} \left(\psi_i^e \right) \left(\frac{\partial \overline{u}}{\partial y} \right) \left(\frac{\partial \psi_j^e}{\partial y} \right) dy, \\ M_{ij}^{21} = 0, M_{ij}^{22} = \int_{y_e}^{y_{e+1}} \left(\psi_i^e \right) \left(\psi_j^e \right) dy, \; M_{ij}^{23} = 0 \end{cases} \tag{24}$$

$$\begin{cases} K_{ij}^{31} = 0, \; K_{ij}^{32} = 0, \\ K_{ij}^{33} = \frac{1}{Sc} \int_{y_e}^{y_{e+1}} \left[\left(\frac{\partial \psi_i^e}{\partial y} \right) \left(\frac{\partial \psi_j^e}{\partial y} \right) \right] dy + \gamma \int_{y_e}^{y_{e+1}} \left(\psi_i^e \right) \left(\psi_j^e \right) dy \\ M_{ij}^{31} = M_{ij}^{32} = 0, M_{ij}^{33} = \int_{y_e}^{y_{e+1}} \left(\psi_i^e \right) \left(\psi_j^e \right) dy \end{cases} \tag{25}$$

$$\begin{cases} b_i^{1e} = 0, b_i^{2e} = \left[\left(\frac{\psi_i^e}{Pr} \right) \left(\frac{\partial \theta}{\partial y} \right) \right]_{y_e}^{y_{e+1}}, \\ b_i^{3e} = \left[\left(\frac{\psi_i^e}{Sc} \right) \left(\frac{\partial \phi}{\partial y} \right) \right]_{y_e}^{y_{e+1}} \end{cases} \tag{26}$$

3.4 Grid Independy Study

In general, to study the grid independency (or) dependency, a grid refinement test is carried out by dividing the whole domain into successively sized grids 81x81, 101x101 and 121x121 in the z-axis direction. Furthermore, we ran the developed code for different grid sizes and finally we found that all the solutions are independent of grid. After many tests, we adopted grid size as 101 intervals. Thus, all the computations were carried out with 101 intervals of equal step size 0.01. At each node 4 functions are to be evaluated and after assembly of element equations, a set of 404 non-linear equations are obtained and which may not produce closed form solutions, consequently an iterative scheme is adopted to solve the system by introducing the boundary conditions. Finally, the solution is assumed to be *convergent whenever the relative difference between two successive iterations* i.e. the iterative process is terminated when the following condition $\sum_{i,j} \left| \xi^{n+1} - \xi^{n} \right| \le 10^{-6}$ where $\xi = u, \theta, \phi$ and n denote the *iterative step*. We also check how the mesh size should be varied at different mesh (grid) sizes and get a range at which there is no variation in the solutions. From table 1, we conclude that no variations in velocity, temperature and concentration. Hence the results are independent of mesh size.

Table 1. The numerical values of u, θ and ϕ for different mesh (grid) sizes at $t = 0.5$

	Mesh size = 0.01			Mesh size = 0.001		
	u	θ	ϕ	u	θ	ϕ
$t = 0.5$	0.3000	0.8200	0.8200	0.3000	0.8200	0.8200
	0.4968	0.7724	0.7951	0.4968	0.7724	0.7951
	0.6733	0.7275	0.7710	0.6733	0.7275	0.7710
	0.8301	0.6852	0.7475	0.8301	0.6852	0.7475
	0.9676	0.6454	0.7247	0.9676	0.6454	0.7247
	1.0867	0.6079	0.7026	1.0867	0.6079	0.7026
	1.1833	0.5392	0.6811	1.1833	0.5392	0.6811
	1.2734	0.5078	0.6603	1.2734	0.5078	0.6603
	1.3430	0.4783	0.6400	1.3430	0.4783	0.6400
	1.3981	0.4504	0.6204	1.3981	0.4504	0.6204
	1.4400	0.4242	0.6013	1.4400	0.4242	0.6013
	1.4696	0.3994	0.5827	1.4696	0.3994	0.5827

Now it is important to calculate the physical quantities of primary interest, which are the Skin-friction, Wall couple stress, Nusselt number and Sherwood number.

Skin-friction is obtained as,

$$\tau = -\left[\frac{\partial u}{\partial y} \right]_{y=0} \tag{27}$$

Nusselt number is obtained as,

$$Nu = -\left[\frac{\partial \theta}{\partial y} \right]_{y=0} \tag{28}$$

Sherwood number is obtained as,

$$Sh = -\left[\frac{\partial \phi}{\partial y} \right]_{y=0} \tag{29}$$

Table 2: Variations of in coefficient of skin friction for different Gr, Gm, M, K

Gr	Gm	M	K	τ
5.0	5.0	1.0	0.5	1.4325
10	5.0	1.0	0.5	1.8304
5.0	**10**	1.0	0.5	2.0432
5.0	5.0	**2.0**	0.5	1.3876

5.0	5.0	1.0	**1.0**	1.7834

Table 3: Variations of in coefficient of skin friction and Nusselt number for different Pr, F, Q, Ec

Pr	F	Q	Ec	τ	Nu
0.71	0.5	1.0	0.001	1.8652	0.4213
1.0	0.5	1.0	0.001	1.4120	1.3025
0.71	**1.0**	1.0	0.001	2.4512	0.5874
0.71	0.5	**2.0**	0.001	1.6314	0.3056
0.71	0.5	1.0	**0.005**	1.7201	0.1104

Table 4: Variations of in coefficient of skin friction and Sherwood number for different Sc, γ

Sc	γ	τ	Sh
0.22	0.5	1.4067	0.5608
0.60	0.5	1.1341	1.0105
0.22	**1.0**	1.2788	0.7338

Tables 2,3,4 show the numerical values of the Skin friction τ, Nusselt number Nu and Sherwood number Sh for various physical parameters involved in the formulation. From table 2, it is observed that Gr, Gm, K increases skin friction increases, whereas the skin friction decreases as M increases. Further, it is noticed from table 3 that as Pr, Q and Ec increases skin friction decreases but in case of F skin friction increases. As Pr, F increases Nusselt number increases and Q, Ec increases Nusselt number decreases. Furthermore, table 4 depicts that as Sc, γ increases skin friction decreases, opposite behaviour is observed in case of Sherwood number i.e. Sc, γ increases Sherwood number increases.

4 Results And Interpretation

The nonlinear boundary value problem solved in the previous section is dictated by an extensive number of thermal and hydrodynamic parameters. To gain a clear insight into the physical problem, numerical calculations for distribution of the velocity, temperature and concentration for different values of these parameters is conducted with graphical illustrations (**Figs. 2-18**). For our computation, we adopted the following default parameters: $a = 1.5, t = 0.5$ and all graphs therefore correspond to these values unless specifically indicated otherwise on the appropriate graph. The permeability in all the Figures plotted is set at 0.5 which corresponds to a highly porous regime, characteristic of many materials operations and working MHD generators. The value of Pr is taken to be 0.71 which corresponds to air at 20°C and 1 atmospheric pressure and the value of Sc is 0.6 (water-vapour). Due to the presence of free convection currents, large positive values of $Gr = 5$ and $Gm = 5$ are selected which imply strong thermal and species buoyancy effects in the regime and where the thermal buoyancy is twice the intensity of species buoyancy.

The influence of angle of inclination (α) of the surface velocity profiles has been depicted in **Figure 2**. It is clearly observed from the figures that velocity is decreased with an increase of angle of inclination, this is since drag is experienced at the plate surface so that it is harder for the fluid to flow along the plate. Furthermore, the buoyancy effects decrease due to the thermal diffusion decrease by a factor of gravity components $\cos\alpha$. Hence the fluid attains high velocity profiles for the vertical plate $(i.e., \alpha = 0^0)$ than that of inclined plate.

Figures 3 and 4 present the effect of thermal radiation-conduction parameter F on respectively linear velocity and temperature profiles. This parameter is defined as $F = 16a^*\nu^2\sigma T_\infty'^3 / \kappa U_0^{\,2}$ and features in the augmented thermal diffusion term in equation. (11). It defines the relative contribution of thermal radiation heat transfer to thermal conduction heat transfer. When $F < 1$ thermal conduction dominates. When $F = 1$ both thermal conduction and thermal radiation contributions are equal. For $F > 1$ thermal radiation dominates over thermal conduction. Fig. 3 clearly reveals that there is a strong deceleration in the linear velocity with increasing F values. The energizing of the flow enhances thermal diffusion but counteracts momentum diffusion. This leads to an increase in momentum boundary layer thickness. Increasing radiation-conduction parameter is also found to decrease temperatures in the boundary layer (fig. 4). Thermal boundary layer thickness is therefore also reduced with greater values of F.

Figures 5 and 6 illustrate the influence of the Eckert number i.e. viscous dissipation parameter (Ec) on velocity and dimensionless temperature profiles. Ec expresses the relationship between the kinetic energy in the flow and the boundary layer enthalpy difference. It embodies the conversion of kinetic energy into internal energy by work done against the viscous fluid stresses. It is an important parameter for describing real working fluids in various materials processing operations where dissipation effects are not trivial. Convection is enhanced and we observe in consistency with that the fluid is accelerated. Temperatures are also enhanced markedly with greater Eckert number, as shown in Figure 6 since internal energy is increased due to kinetic energy dissipation.

Figures 7 and 8 depicts the influence of heat absorption parameter, Q on velocity and temperature distribution respectively in the flow. The heat absorption parameter Q appearing in (2) quantifies the amount of heat absorbed per unit volume which is given by $Q'\left(T_W' - T_\infty'\right)$, Q' being a constant coefficient, which may take as either positive or negative or zero (no heat source./sink). The source term represents heat absorption for $Q > 0$ and heat generation when $Q < 0$. Physically speaking, the presence of heat absorption (thermal sink) effects has the tendency to reduce the fluid temperature. This de-energizes the flow and causes a strong deceleration i.e. net reduction in the fluid velocity, as observed in Fig. 7. Greater

heat absorption Q clearly reduces the temperatures in the domain as observed in Fig. 8, and the effect is most prominent at the wall.

Figures 9 and 10 illustrate the influence of Prandtl number (Pr) on the linear velocity and temperature profiles. With greater Prandtl number the velocity is significantly decreased throughout the boundary layer as in fig 9. Prandtl number represents the relative rate of momentum diffusion to energy diffusion. With Pr > 1 the momentum diffusion rate also exceeds the thermal diffusion rate in the fluid. This will also manifest in an increase in momentum (hydrodynamic) boundary layer thickness. Similarly, there is a strong depression in temperature with greater Prandtl number (Pr), greater Prandtl number corresponds to a lower thermal conductivity. This leads to a reduction in thermal energy convected through the fluid from the plate (Gr >0 i.e. plate cooling) and depresses the thermal boundary layer thickness.

Figure 11 and 12 illustrates the response of velocity and concentration profiles to different values of Schmidt number (Sc). The Schmidt number is a fundamental parameter in species diffusion (mass transfer) which describes the ratio of the momentum to the molecular (species) diffusivity i.e. $Sc = v / D$. The Schmidt number therefore quantifies the relative effectiveness of momentum and mass transport by diffusion in the hydrodynamic (velocity) and concentration (species) boundary layers. It is observed that as the Schmidt number increases both velocity and concentration decreases. The momentum boundary layer thickness is also *reduced* with greater Schmidt number. The associated decrease in species diffusivity results in less vigorous mass transfer which reduces concentration levels and depletes the concentration boundary layer thickness. Mass transfer therefore exerts interplay with the velocity field and the distribution of species in materials can be manipulated via the Schmidt number.

Figures 13 **and 14** illustrate the evolution in velocity and concentration with a change in chemical reaction parameter (γ). The reaction parameter is based on *a first-order irreversible chemical reaction* which takes place both in the bulk of the fluid (homogeneous) as well as at plate which is assumed to be catalytic to chemical reaction. We consider the *destructive type* of homogenous chemical reaction. Increasing γ values are found, in fig. 13, to instigate a considerable reduction in the velocity i.e. flow deceleration. Fig. 14 shows that concentration is also depleted in the boundary layer with greater chemical reaction, since more species is destroyed via the chemical reaction. This results in a reduction in the thickness of the concentration boundary layer.

Figures 15-16 depict the evolution in velocity with different thermal Grashof Gr and species Grashof Gm numbers. Both Grashof numbers arise solely in the thermal and species buoyancy terms in the normalized momentum conservation eqn. (10) i.e. $+Gr\theta$, $+Gm\phi$ .Thermal Grashof number Gr is described here as quantifying the relative magnitude of the thermal buoyancy force and the opposing viscous hydrodynamic (frictional) force acting on the Newtonian fluid. The velocity profiles are invariably enhanced with an increase of *positive* thermal Grashof number (the only case studied). For $Gr >1$ there is a dominance of buoyancy forces over the viscous forces, which in turn further accelerates the flow (Fig. 15). Increasing thermal buoyancy is therefore assistive to momentum development and results in a *decrease* in momentum boundary layer thickness. Fig. 16 shows that an increase in species (solutal) Grashof number Gm in fact generates an even greater acceleration in the flow and substantially elevates velocity (u) throughout the boundary layer. The increasing concentration gradient associated with higher Gm values accentuates the species buoyancy force which adds driving potential to the boundary layer flow and manifests again in acceleration and decreasing momentum boundary layer thickness.

Figure 17 shows the pattern of the velocity for different values of magnetic field parameter M . It is observed that the amplitude of the velocity as well as the boundary layer thickness decreases when M is increased. Physically, it may also be expected due to the fact that the magnetic field exerts a retarding effect on the free convective flow and upon increasing the values of M , this type of resisting force slows down the fluid, hence it is obvious that the effect of increasing values of the parameter M results in a decreasing velocity distribution across the boundary layer.

The profiles of the velocity in the boundary layer for various values of the permeability K are shown in **Figure 18**. It is seen that the peak value of the velocity near the wall of the porous plate increases rapidly with K .It is seen also that the microrotation increases with increase in K .

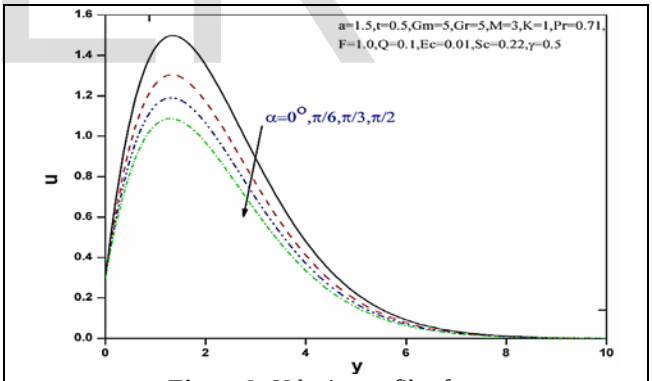

***Figure 2**: Velocity profiles for α*

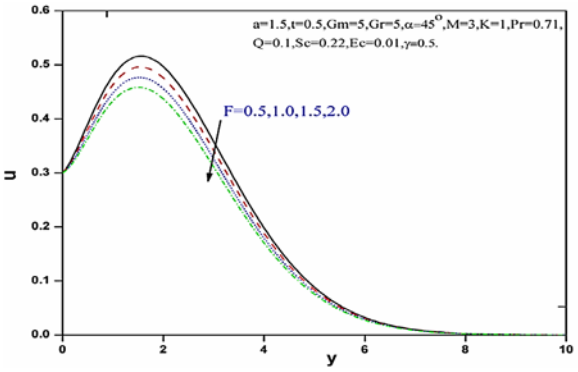

***Figure 3**: Velocity profiles for F*

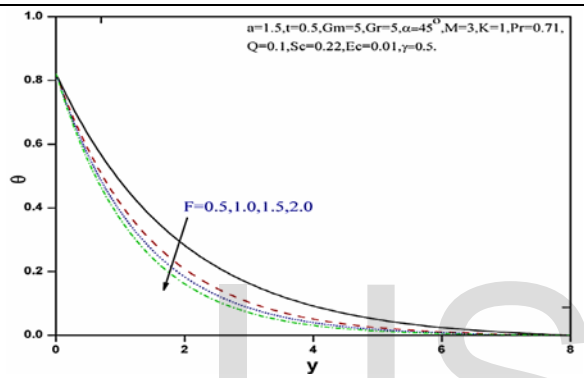

***Figure 4:** Temperature profiles for F*

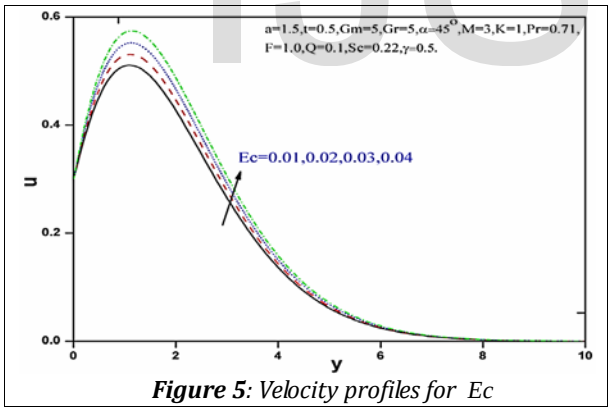

***Figure 5**: Velocity profiles for Ec*

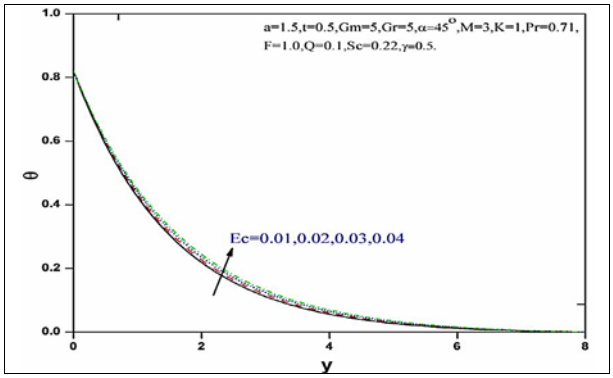

Figure 6: Temperature profiles for *Ec*

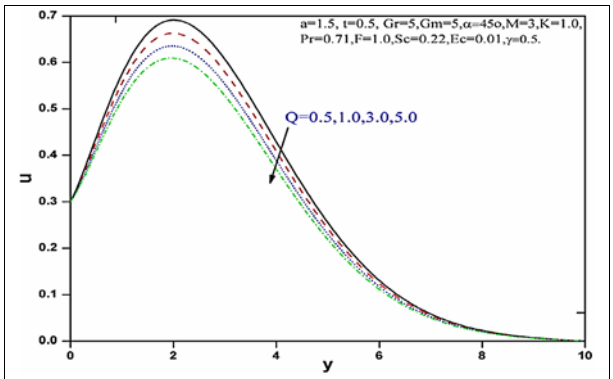

***Figure 7**: Velocity profiles for Q*

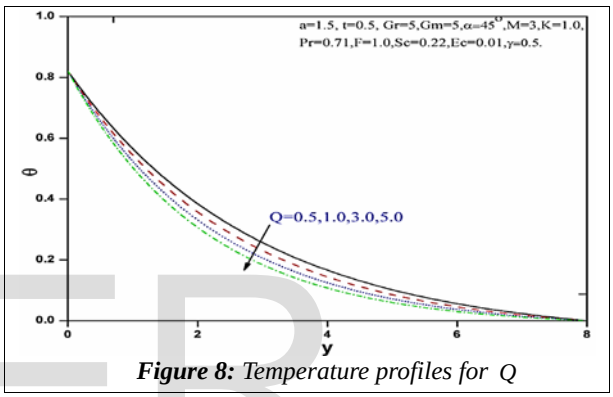

***Figure 8:** Temperature profiles for Q*

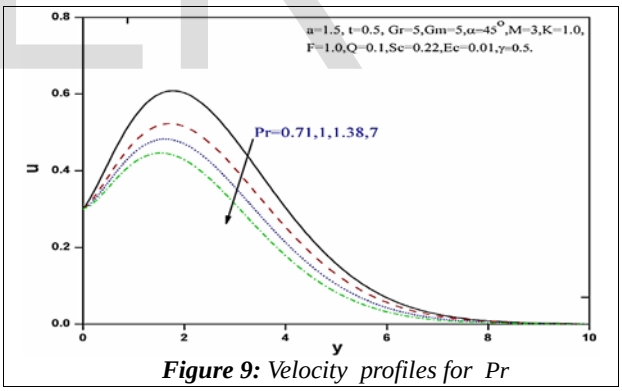

***Figure 9:** Velocity profiles for Pr*

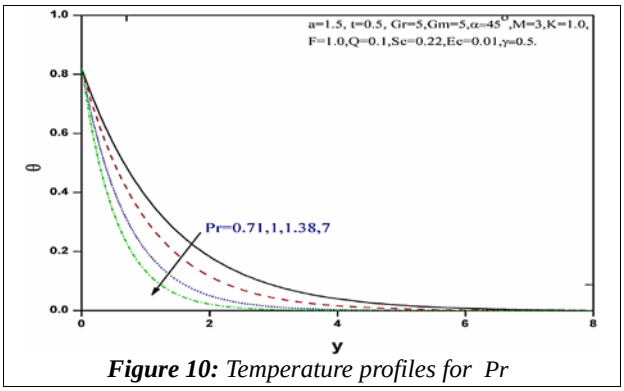

***Figure 10:** Temperature profiles for Pr*

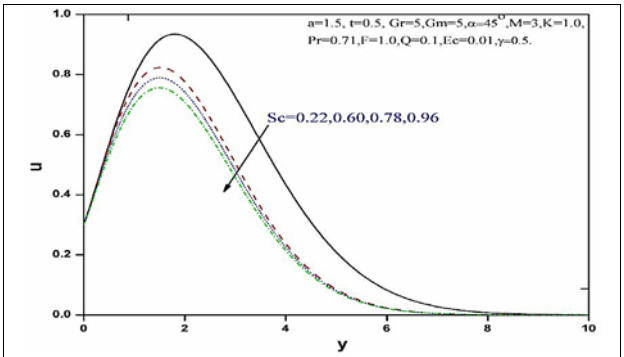

Figure 11: *Velocity profiles for Sc*

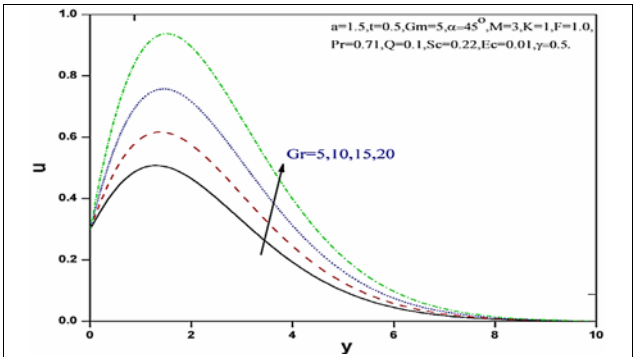

Figure 15: *Velocity profiles for Gr*

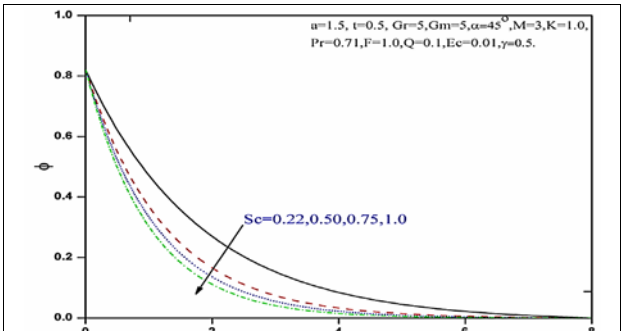

Figure 12: *Concentration profiles for Sc*

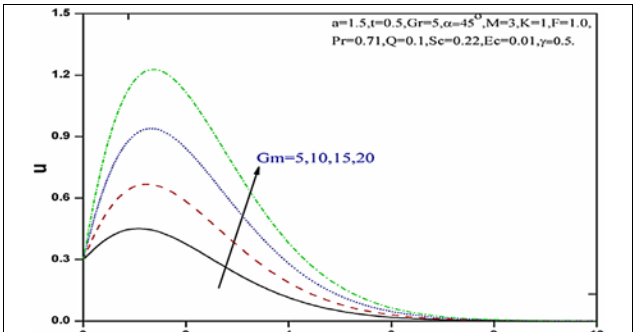

Figure 16: *Velocity profiles for Gm*

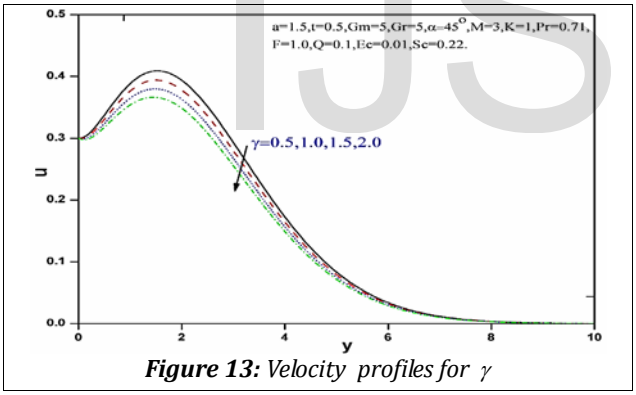

Figure 13: *Velocity profiles for* γ

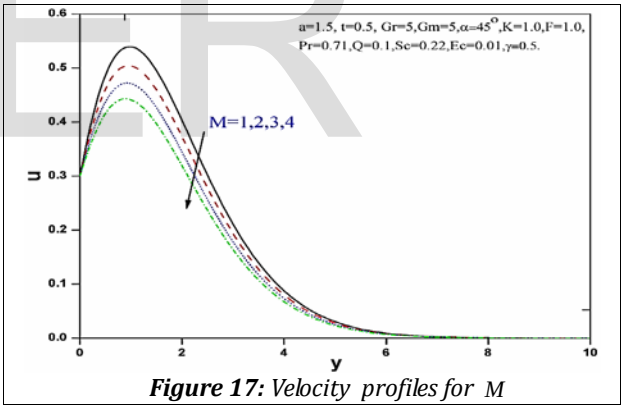

Figure 17: *Velocity profiles for M*

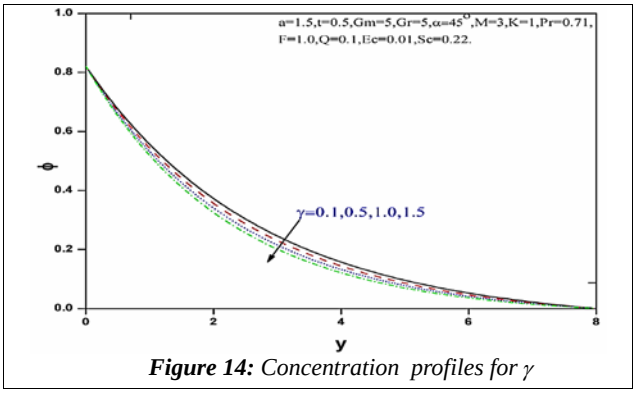

Figure 14: *Concentration profiles for* γ

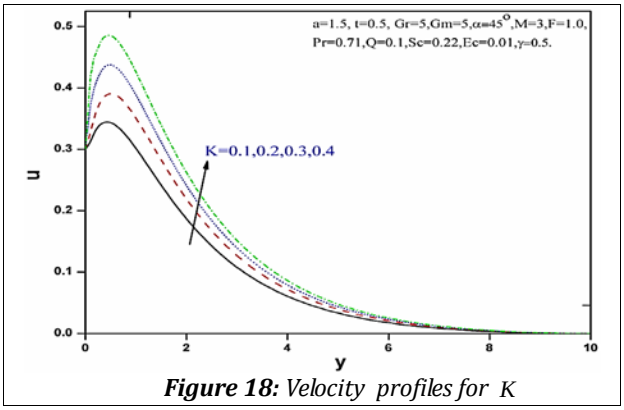

Figure 18: *Velocity profiles for K*

5 Conclusions

Motivated by the previous works and possible applications, the finite element solution has been developed for Effects of Thermal radiation and viscous dissipation on unsteady free magneto convective heat and mass transfer in newtonian fluid flow from an inclined porous plate. We investigated, how the flow field, temperature and concentration field are affected by the variations of the Magnetic parameter M ,Thermal radiation parameter F ,Eckert number Ec ,Heat absorption parameter Q , angle of tion α ,Permeability of porous medium K , Prandtl number Pr , Schmidt number Sc , Grashof number Gr , Modified Grashof number Gm and Chemical reaction parameter γ and discussed the results.From the Present numerical study the final remarks can be listed as follows:

1. The flow is decelerated and momentum boundary layer thickness increased with increasing values of angle of inclination, magnetic body force parameter, Prandtl number,Thermal radiation parameter, heat absorption parameter,Schimdt number and chemical reaction parameter.
2. The flow is acelerated and momentum boundary layer thickness decreased with increasing values of permeability parameter, thermal Grashof number and species Grashof number, Eckert number.
3. An increase in viscous dissipation parameters accelerates the thickness thermal boundary layer but a reverse phenomenon is observed in Prandtl number, Thermal radiation and heat absorption.
4. An increase in physical parameter Schmidt number and homogeneous chemical reaction parameter to decrease in thickness of concentration boundary layer.

References

[1] O. Anwar Beg, "Numerical methods for multi-physical magnetohydrodynamics, New Developments in Hydrodynamics Reaserch," Maximiano J. Ibragimov and A. Anisimov, Eds., Ch.1, pp.1-110, 2012, Nova Science, Newyork.

[2] G.J. Womack, "*MHD Power Generation*". London: Chapman and Hall, 1969.

[3] A. Postelnicu, "Influence of a magnetic field on heat and mass transfer by natural convection from vertical surfaces in porous media considering Soret and Dufour effects," Int. J. Heat and Mass Transfer. **47**, 1467-1472, 2004.

[4] T. Hayat, R. Naz, A. Alsaedi, M.M. Rashidi, "Hydromagnetic rotating flow of third grade fluid," Appl. Math. Mech. **34** (12), 1481-1494, 2013.

[5] R.A. Mohamed, A.N.A. Osman, S.M. Abo-Dahab, "Unsteady MHD double-diffusive convection boundary layer flow past a radiate hot vertical surface in porous media in the presence of chemical reaction and heat sink," Meccanica. **48**, pp.931–942, 2013.

[6] F.I. Alao, A.I. Fagbade, B.O. Faludon, "Effect of thermal radiation, Soret and Dufour on an unsteady heat and mass transfer flow of a chemically reacting fluid past a semi-infinite vertical plate with viscous dissipation," J.Nigerian.Math.Soc.,2016. http://dx.doi.org/10.1016/j,jnnms.2016.01.002.

[7] N. Ali, S.U. Khan, Z. Abbas, M. Sajid, "Soret Dufour effects on hydromagnetic flow of visco elastic fluid over porous oscillatory stretching sheet with thermal radiation," J. Braz. Soc. Mech. Sci. Eng. (2016). doi: 10.1007/s40430-016-0506-x.

[8] S. Ahmed, A. Batin, A.J. Chamkha, "Finite difference approach in porous media transport modelling for magnetohydrodynamics unsteady flow over a vertical plate: Darcian Model. Int. J. Numerical Method for Heat and Fluid Flow," 24 (5), pp.1-12, 2014. doi: 10.1108/HFF-01-2013-0008.

[9] R. Sharma, R. Bhargava, P. Bhargava, "A Numerical solution of unsteady MHD convection heat and mass transfer past a semi-infinite vertical porous plate using element free Galerkin method," Comput. Mat. Sci., **48**, 537-548, 2010. doi: 10.1016/j.commatsci.2010.02.020

[10] K.A. Helmy, "Unsteady free convection flow past a vertical porous plate," *ZAMM.Z.* Agnew.Math.Mech. **78(4),** pp. 255-270, 1998.

[11] V.M. Soundalgekar, S.K. Gupta, N.S. Birajdar, "Effects of mass transfer and free effects on MHD stokes problem for a vertical plate," Nuclear Eng. Des, **53**, pp. 309-346, 1979.

[12] M. Umamaheshwar, M.C. Raju, S.V.K. Varma, "Analysis of MHD transient free convection flow of a Newtonian fluid pas an infinite vertical porous plate," Frontiers in Heat and Mass Transfer. **18 (6)**, 2015. doi:10.5098/hmt.6.18.

[13] B. Rushi Kumar, T. Sravan Kumar, A.G. Vijaya Kumar, "Thermal diffusion and Radiation effects on unsteady free convection flow in the presence of Magnetic fixed relative to the fluid or to the plate," *Frontiers in Heat and Mass Transfer* **12(6)**, 2015. doi:10.5098/hmt.6.12.

[14] E.M. Sparrow, R. Eichhorn, J.L. Grigg, "Combined and Free Convection in a Boundary Layer," Physics of Fluids 2, pp. 319-320, 1959.

[15] B. Gebhert, L. Pera, "The nature of vertical natural convection flows resulting from Combined Buoyancy effects of thermal and mass diffusion," Int. J. Heat Mass Transfer. **14,** pp. 2025-2050, 1971.

[16] T.S. Chen, C.F. Yuh, "Combined heat and mass transfer in mixed convection along vertical and inclined plates," Int. J. Heat Mass Transfer. **23**, pp. 527-537, 1980.

[17] A.J. Chamkha, A.R.A. Khaled, "Similarity solutions for hydromagnetic simultaneous heat and mass transfer by natural convection from an inclined plate with internal heat generation or absorption," Heat and Mass Transfer. **37,** pp. 117-123, 2001.

[18] P.K. Singh, "Heat and Mass Transfer in MHD Boundary Layer Flow past an Inclined plate with Viscous Dissipation in Porous Medium," Int. J. Scientific Eng. Reaserch. **3(6),** pp. 2229-5518, 2012.

[19] P. Cheng, "Combined free and forced convection flow about inclined surfaces in porous media," Int. J. Heat Mass Transfer. **20**, pp. 807-814, 1977.

[20] C.H. Chen, "Heat and mass transfer in MHD flow by natural convection from a permeable inclined surface with variable wall temperature and concentration," Acta Mechanica. **172**, pp. 219-235, 2004.

[21] M.F. Modest, "*Radiative Heat Transfer*," Second ed., Academic Press, 2003, New York.

[22] R. Siegel, J.R. Howell, "*Thermal Radiation Heat Transfer*," Fourth ed., Taylor & Francis, 2002, New York.

[23] R. Muthucumaraswamy, G. Kumar Senthil, "Heat and Mass transfer effect on moving vertical plate in the presence of thermal radiation," Theoret. Appl. Mech. **31,** 35, 2004.

[24] B. Gebhert, "Effect of viscous dissipation in natural convection," J. Fluid Mech. **14**, pp. 225-232, 1962.

[25] V.A.F. Costa, Thermodynamics of natural convection in enclosures with viscous dissipation. Int. J. Heat and Mass transfer, **48**, pp. 2333-2341, 2005.

[26] M. Gnaneswara Reddy, N. Bhaskar Reddy, "Radiation and mass transfer effects on unsteady MHD free convection flow past a vertical porous plate with viscous dissipation," Int. J. Appl. Math. Mech. **6 (6)**, pp. 96–110, 2010.

[27] S. Sivaiah, R. Srinivasa raju, "Finite element solution of heat and mass transfer flow with hall current, heat source and viscous dissipation," Appl. Math. Mech. -Engl. Ed.2013, **34**, pp.559–570, 2013.

[28] M.S. Babu, P.V. Satya Narayana, "Effects of the chemical reaction and radiation absorption on free convection flow through porous

medium with variable suction in the presence of uniform magnetic field," J. of Heat and Mass Transfer, **3**, pp. 219–234, 2009.

[29] R. Nandkeolyar, M. Das, P. Sibanda, "Unsteady hydromagnetic heat and mass transfer flow of a heat radiating and chemically reactive fluid past a flat porous plate with ramped wall temperature," Mathematical Problems in Engineering. Article ID 381806. 2013.

[30] G.S. Seth, R. Sharma, R., and S.M. Hussain, "Hall effects on unsteady MHD natural convection flow of heat absorbing fluid past an accelerated moving vertical plate with Ramped temperature," Emirates Journal of Engineering Reaserch. **19**, pp. 19-32, 2014.

[31] S. Siva Reddy, MD. Shamshuddin, "Heat and mass transfer on the MHD flow of a micropolar fluid in the presence of viscous dissipation and chemical reaction," Procedia. Eng., **127**, pp. 885-895, 2015.

[32] S. Siva Reddy, MD. Shamshuddin, "Diffusion-thermo and chemical reaction effects on an unsteady MHD free convection flow in a micropolar fluid," Theoret. Appl. Mech., **43,** pp. 117-131, 2016.

[33] K.R. Cramer, S.I. Pai, "*Magneto fluid Dynamics for Engineers and Applied Physicists*," *McGraw- Hill*, 1973, New York, USA.

[34] A.C. Cogley, W.G. Vinceti, S.E. Gilles, "Differential approximation for radiation transfer in a non-grey near equilibrium," AIAA Journal. 6, pp. 551-553, 1968.

[35] T. Hayat, M. Mustafa, M. Sajid, "Influence of thermal radiation on Blasius flow of a second-grade fluid," Z Naturforsch, **64a,** pp. 827–833, 2009.

[36] A. Pantokratoras, T. Fang, "Blasius flow with non-linear Rosseland thermal radiation," Mechanica. **49,** pp.1539-1545, 2014.doi:10.1007/s11012-014-9911-3.

[37] J.N. Reddy, "*An Introduction to the Finite Element Method*," McGraw-Hill Book Company, New York 3rd Edition, 2006.

[38] K. J. Bathe, "*Finite element procedures*," Prentice Hall, 1996, New Jersy, USA.